

NONLINEAR DYNAMIC RESPONSES OF LOCOMOTIVE EXCITED BY RAIL CORRUGATION AND GEAR TIME-VARYING MESH STIFFNESS

Zaigang CHEN¹, Jie ZHANG², Kaiyun WANG^{3*}, Pengfei LIU⁴

^{1,2,3}State Key Laboratory of Traction Power, Southwest Jiaotong University, Chengdu, China

⁴School of Mechanical Engineering, Shijiazhuang Tiedao University, Shijiazhuang, China

Submitted 22 August 2017; resubmitted 8 November 2017, 23 April 2018; accepted 4 July 2018

Abstract. Rail corrugation is usually generated in modern railway transportations, such as high-speed railway, urban railway, and heavy-haul railway. It is one of the major excitations to the wheel–rail dynamic interaction, which will cause extra vibration and noise, failures, or even risk of derailment to the vehicle and its components. A dynamics model of a heavy-haul locomotive considering the traction power from the electric motor to the wheelset through gear transmission is employed to investigate the nonlinear dynamic responses of the locomotive. This dynamics model couples the motions of the vehicle, the track, and the gear transmission together. In this dynamics model, excitations from the rail corrugation, the nonlinear wheel–rail contact, the time-varying mesh stiffness, and the nonlinear gear backlash are considered. Then, numerical simulations are performed to reveal the dynamic responses of the locomotive. The calculated results indicate that different nonlinear phenomenon can be observed under the excitation of the rail corrugation with different amplitude and wavelength. The high frequency vibrations excited by the time-varying mesh stiffness are usually modulated by the low frequency vibrations caused by the rail corrugation. However, this is likely to vanish under the chaotic conditions with some corrugation wavelength. The vibration level of the vehicle and the gear transmission increases generally with the corrugation amplitude. However, some corrugation lengths have been found to be more responsible for the vibration of the dynamics system, which should be concerned greatly during the locomotive operation. Meanwhile, involvement of gear transmission systems will cause different dynamic responses between the wheelsets under rail corrugation and gear mesh excitations.

Keywords: nonlinearity, rail corrugation, mesh stiffness, gear backlash, dynamic response, railway vehicle.

Notations

BSC – backward-side contact;
DOF – degrees of freedoms;
DTE – dynamic transmission error;
FSC – forward-side contact;
LOA – line of action;
RMS – root mean square.

Introduction

Rail corrugation has troubled the railway company and scholars for more than a century due to its complicated mechanism of formation and diversity of characteristics. Even until now, its formation mechanism is still confusing the people throughout the world even if there has been plenty of research work on this subject. Consequently, it has brought lots of research topics to the related scholars worldwide, such as investigations of the rail corrugation

formation mechanism and the technologies and methods for its measurement and treatment.

Grassie and Kalousek (1993) identified 6 types of rail corrugations by their 2 critical characteristics, namely the wavelength-fixing mechanism that gives rise to the periodicity, and the damage mechanism that causes the perceived damage. In their work, the corresponding treatment or measurement of preventing rail corrugation were also introduced. Then, Sato *et al.* (2002) reviewed the major research team and their main work on the formation mechanism of rail corrugations, and found some of the rail corrugations had not been understood clearly yet. And Grassie (2009) identified further the 6 types of the rail corrugations based on the updated knowledge and understanding in the formation mechanism of the rail corrugations since 1993, where 2 types of rail corrugations, namely the “booted sleepers” and the “contact fatigue”,

*Corresponding author. E-mail: kywang@home.swjtu.edu.cn

were replaced by “other P2 resonance” and “trackform-specific”, and the pinned-pinned resonance was demonstrated as the wavelength-fixing mechanism for the corrugations of “roaring rails”. Correa *et al.* (2011) investigated the rail corrugation wear on 4 types of high-speed tracks by establishing a numerical model that integrated the coupled dynamics model of the track and the wheelset with the wear mechanism model. Recently, Li *et al.* (2017) supplied some new insights into the short pitch corrugation development enigma by coupling the wheel–rail contact mechanics with the structural dynamics in a vehicle-track system. They found the longitudinal vibration modes play a major role in the short pitch corrugation initiation, and the consistency between the longitudinal and the vertical modes determines the corrugation evolution.

As is known that, presence of the rail corrugation will inevitably exacerbate the dynamic performance of both the vehicle system and the track system by increasing the wheel–rail dynamic interactions. Studies on effect of the rail corrugation on the dynamic performance of the coupled vehicle–track dynamics system have drawn great attentions worldwide, which are also foundations for revealing the rail corrugation formation mechanism and developing the technologies and methods for rail corrugation measurement and treatment. In previous published literatures, there are some effective dynamics models for the vehicle–track system, which enables the simulation under the wheel–rail excitations such as the rail corrugation. One of these typical models, namely the “Zhai model”, was firstly proposed (Zhai, Sun 1994; Zhai *et al.* 2009). In their work, the vehicle and the track were coupled as an integral system through the wheel–rail contact interface, which has proven to be a more complete model for the railway dynamics and has been employed widely in solving practical engineering problems by the following researchers. Shabana and Sany (2001) made a review on the development of the dynamic models for railroad vehicle and track system and suggested the inclusion of adopting computational flexible multibody methodologies would bring benefits in the railroad vehicle/track dynamic simulations. Matsumoto *et al.* (2002) performed many full-scale stand tests, commercial line experiments and numerical simulations, and indicated that the corrugation of rail in curve section of track is caused by wheel–rail stick–slip vibration due to the large creepage and vertical force fluctuation on wheel–rail contact interface. Ling *et al.* (2014) investigated the effect of the rail corrugation on the dynamic behaviour of the rail fastening for a metro line by experimental test and numerical simulation. Wang *et al.* (2015) performed studies on the effect of rail corrugation in a high-speed railway on the wheel–rail dynamic interactions, where the rail corrugations with different wavelength and depth were analysed to search the sensitive wavelength.

Most of these literatures disregarded the dynamic effect from the mechanical transmission system including the gear mesh excitations in the powered vehicle, such as a locomotive. However, the flexible deformations of the

mechanical transmission will have an apparent effect on the oscillation of the wheel–rail contact force, especially when the time-varying mesh stiffness of the gear pairs in the mechanical transmission systems are considered. In addition, in reverse, the rail irregularity such as the periodic rail corrugation will excite not only the vibration of the vehicle–track system but also the vibration of the components in the mechanical transmission system for a locomotive. This dynamic interactions between the wheel–rail contact excitation and the geared mechanical transmission have been revealed by Chen *et al.* (2017a, 2017b) who developed more complete vehicle–track coupled dynamics models with consideration of geared mechanical transmissions. Their model is capable of performing dynamic simulations on the locomotive–track coupled system under both the nonlinear wheel–rail excitations (e.g., rail corrugation) and the gear mesh excitation (e.g., time-varying mesh stiffness).

Time-varying mesh stiffness is one of the inherited characteristics of gear pairs that excite the vibration of the gear transmission system. Thus, it has attracted so much attention from the scholars. For example, Weber (1951) developed an analytical model for calculation of the loaded gear tooth deformation, where 3 parts, namely the basic tooth deformation, the fillet–foundation deformation and the contact deflection were included. Chaari *et al.* (2009) developed an analytical model of gear mesh stiffness based on the Weber’s model. Tian (2004) and Wu *et al.* (2008) refined the calculation model of total mesh stiffness for spur gear pairs developed by Yang, Lin (1987) based on the potential energy principle. And then the model was extended by Chen, Shao (2011, 2013); Chen *et al.* (2016); Shao, Chen (2013), where the fillet–foundation deflection (Sainsot *et al.* 2004; Chen *et al.* 2017c) was considered and the gear tooth was regarded as a non-uniform cantilever beam attached to the root circle. This theory is also widely employed by other researchers in their research work, such as Ma *et al.* (2015) and Liang *et al.* (2014).

In this paper, a locomotive–track coupled dynamics model proposed in our previous work (Chen *et al.* 2017b) is employed to investigate the locomotive dynamic characteristics. The main contribution of this paper is to reveal the effects of both the rail corrugation excitations with different wavelength and amplitude and the time-varying mesh stiffness excitations the on the vibration responses of the locomotive dynamics system, especially for the gear transmission system. This work could be hardly found in the previously published literatures. Besides, this work supplies a possible method for dynamic assessment of gear transmissions in the vibration environment of the entire locomotive–track coupled dynamics system under the excitations of rail corrugation. Some assumptions are made as:

- » the rail corrugations contribute mainly to the variations of the wheel–rail vertical and longitudinal dynamic forces, where the lateral motions are negligible;
- » the effect from the variations of the motor electrical

system is so small to be ignored, thus the electro-mechanical interactions are not considered;

»» the wheel–rail adhesion characteristics represented by Equation (2), which is widely used by many scholars can be suitable for the rail corrugation conditions.

This paper is organized as follows: related literatures are reviewed in the section of Introduction, which is followed by section 1 where the locomotive–track coupled dynamics model and the numerical integration method are presented. Based on the developed model, numerical simulation and detailed result discussion are performed in section 2. Finally, some concluding remarks are given out in the last section.

1. Locomotive–track coupled dynamics model considering mechanical transmissions

Locomotives are usually driven by the traction motors whose torques are transmitted to the wheel–rail contact interface for generation of traction forces. In the power transmission path from the motor to the wheelset, gear transmission system is a very vital component. At the vibration point of view, it is also an excitation source generated by its inherited time-varying mesh stiffness due to the variations of the number of teeth in mesh and the variations of the contact position on tooth profile. It has been demonstrated that the gear time-varying mesh stiffness has apparent impact on the vibrations of locomotive–track coupled dynamics system (Chen *et al.* 2017a). Consequently, the mechanical transmission system including gear transmission should be considered to be coupled with the locomotive–track dynamics system, and this model has been developed by Chen *et al.* (2017a, 2017b). In this

paper, this dynamics model is also employed for dynamic simulation. Besides, the longitudinal vibrations of the components in the locomotive are also considered because the traction forces at the wheel–rail contact surfaces need to be transmitted to overcome the resistance during operation, thus they also affect the dynamic performance of the locomotive.

1.1. Nonlinear wheel–rail interactions and rail corrugation excitations

The locomotive–track coupled vertical-longitudinal dynamics model considering the effect of the gear transmission systems is shown in Figure 1. The locomotive in this model is composed of a car body, 2 bogies, and 4 wheelsets with each mounted with a motor and a gear. The car body is supported by 2 bogies through the secondary suspensions, namely the spring–damper (K_{sz}, C_{sz}) elements. While the bogie is carried by 2 wheelsets through the primary suspensions represented by (K_{pz}, C_{pz}). The motor and the gearbox are connected with each other rigidly through bolts, and are suspended by axle-hung bearings (K_{br}, C_{br}) and the hanger rod (K_{ms}, C_{ms}). In this dynamics model, the lumped parameter method is employed, namely all the components (e.g., car body, bogie frames, wheelsets, and motors) are regarded as rigid bodies whose mass M_k and moment of inertia J_k are lumped to their gravity center. 3 DOF, namely the rotational β_k , the vertical Z_k , and the longitudinal X_k motions are considered for each of the rigid bodies. Here, the subscripts ($k = m, w, t, c$) correspond to the motor, the wheelset, the bogie frame, and the car body, respectively.

The total weight of the locomotive is carried by the track structures through the wheel–rail contact. In this pa-

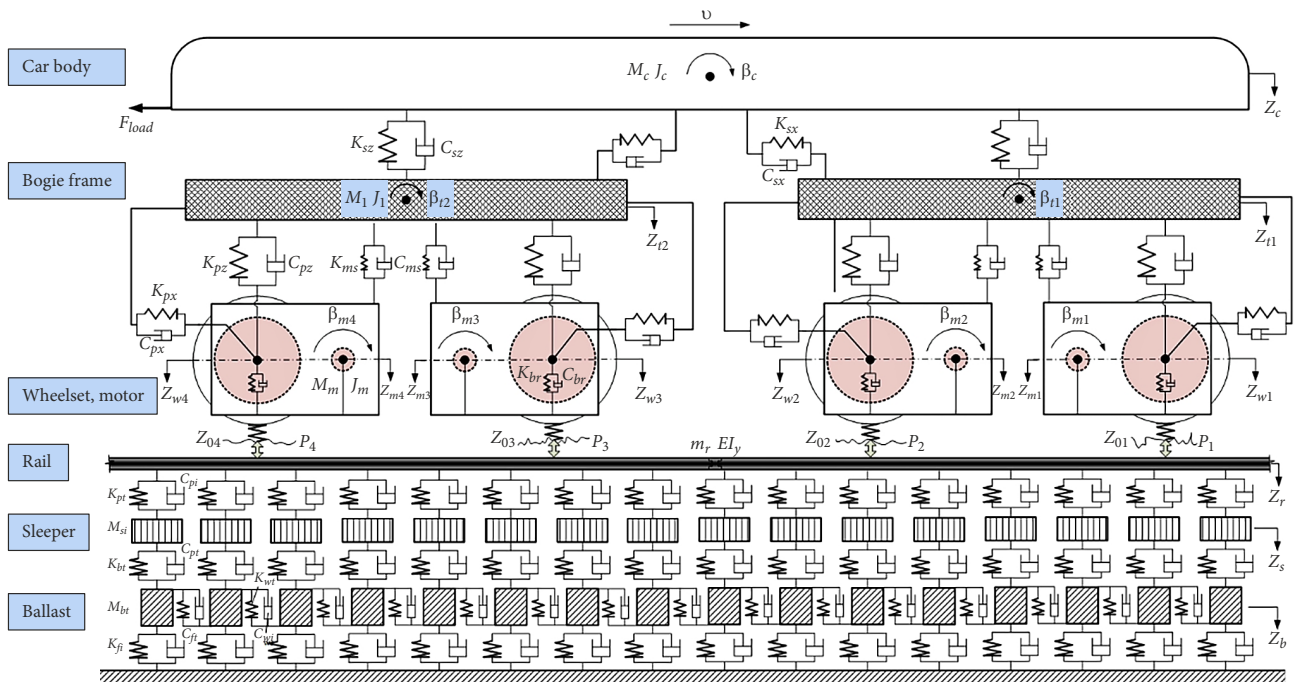


Figure 1. Locomotive–track vertical-longitudinal coupled dynamics model with geared mechanical transmissions

per, a typical ballasted track structure is adopted for simulation, which is shown in Figure 1. The ballasted track structure consists of 4 layers, namely the rail, the sleeper, the ballast, and the rigid subgrade. The elasticity and the damping of the rail pad, the ballast and the subgrade are lumped to a series of spring–damper elements. A series of shear stiffness–damper elements are used to consider the coupling effect of the interlocking ballast granules. More detailed discussions can be found in previous work (Zhai, Sun 1994; Zhai et al. 2009).

The locomotive is finally actuated to move along the track by the creep forces at the wheel–rail contact interfaces. These forces also act as the load to the mechanical transmissions including the motor, the gear pair, and the wheelset. The creep force F_{creep} is calculated by the production of the normal contact force and the adhesion coefficient. It is given as:

$$F_{creep} = P(t) \cdot \mu, \quad (1)$$

where: $P(t)$ denotes the normal wheel–rail contact force; μ is the adhesion coefficient of the wheel–rail contact interface. The equation for μ adopted by Ishikawa and Kawamura (1997) is also used here which is depicted as:

$$\mu = c \cdot \exp(-a \cdot v_s) - d \cdot \exp(-b \cdot v_s), \quad (2)$$

where: the coefficients a , b , c , and d are used to determine the variations of the adhesion coefficient versus the relative slip velocity v_s . The relative slip velocity can be obtained as:

$$v_s = \dot{\theta}_w \cdot R - v_w, \quad (3)$$

where: $\dot{\theta}_w$, R and v_w denote the angular velocity, the radius of the wheel, and the longitudinal velocity of the wheelset, respectively.

This simple form of adhesion coefficient in Equation (2) was obtained by the statistical method based on plenty of theoretical and experimental analysis by lots of scholars, such as Kalker, Piotrowski (1989); Iwnicki (2003); Polach (2005). It should be mentioned that there also exists apparent discrepancy between the experimental test results and the theoretical results since the experimental test results have greater dispersions, which are very difficult to be captured precisely by the theoretical models. The more complicated variation of the adhesion coefficient in practice due to many unknown influencing factors is likely to cause more complex dynamic responses than the simple form of adhesion coefficient used in this study, which requires the development of more detailed and precise creep force calculation methods in the future.

In this paper, the wheel–rail normal contact force is calculated by using the Hertzian nonlinear elastic theory, which is calculated as (Zhai, Sun 1994; Zhai et al. 2009):

$$P(t) = \left(\frac{1}{G} \cdot \delta Z(t) \right)^{\frac{3}{2}}, \quad (4)$$

where: G is a constant wheel–rail contact parameter; $\delta Z(t)$

denotes the elastic compressive deformation of the wheel–rail contact, which is given as:

$$\delta Z(t) = Z_w(t) - Z_r(x_w, t) - Z_0(t), \quad (5)$$

where: Z_w , Z_r represent the vertical displacement of the wheel and the rail at the contact position; $Z_0(t)$ denotes the geometrical irregularities at the wheel–rail contact interface, such as the rail corrugations.

1.2. Time-varying mesh stiffness excitation of gear transmissions in the locomotive

Gear transmission system is an essential element in most of the locomotives for transmission of the forces and motions between the motor and the wheels. The magnetic torque generated between the rotor and the stator of the motor is usually transmitted to the wheel–rail contact interface through the gear teeth engagement so as to produce the tractive forces to make the locomotive to run. The mechanical transmission path, namely the rotor → coupling → pinion → gear → wheel axle → wheel, is shown in Figure 2a. A schematic illustrating the mesh process of the gear transmission is shown in Figure 2b where the 2 circles indicate the base circles of the pinion and the gear, respectively. The flexible deformations of the gear pair in mesh are lumped to the deformations of the spring–damper element (K_m , C_m) along LOA. Under some circumstances with vibrations in huge amplitude, e.g., the light load, resonance vibration, or wheel–rail slippage, the tooth contact lose or even backward-side impact is likely to happen to the gear pair. The solid and dashed LOAs in Figure 2b indicate the FSC and BSC, respectively, for the

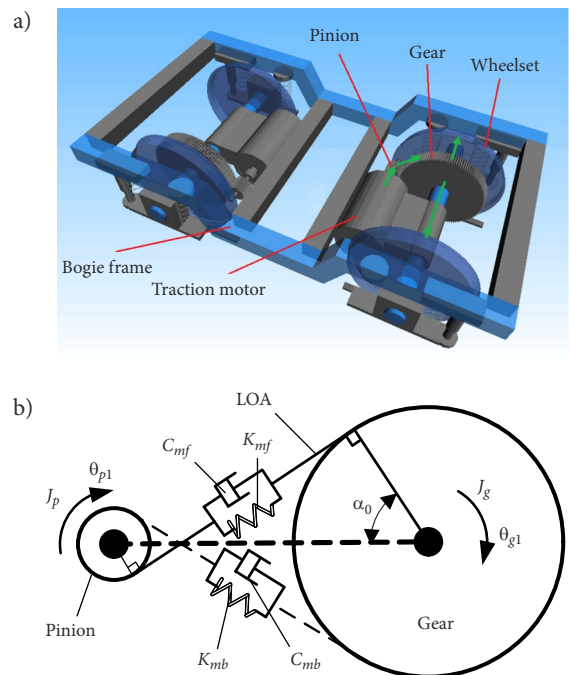


Figure 2. Schematic of mechanical transmission in the locomotive: a – mechanical transmission systems in a bogie; b – dynamic model of gear transmission

gear transmission. Once the tooth contact lose or even the BSC happens, serious impact forces between the gear teeth may be generated. Besides, direction of the gear mesh forces will be altered when the BSC happens. Variations of both the amplitude and the direction of the mesh force will lead to great change of the dynamic responses of the locomotive due to the huge impact dynamic mesh forces to the gear pairs and their connected components, which will increase the risk of failure (Chen *et al.* 2012).

According to the structural characteristics shown in Figures 1 and 2, the DTE representing the compressive deformations of the gear pair could be obtained as:

$$\delta_i = \begin{cases} eqs_1, & \text{for FSC;} \\ eqs_2, & \text{for BSC;} \end{cases} \quad (6)$$

$$\begin{aligned} eqs_1 = & -R_p \cdot \theta_{pi} - R_g \cdot \theta_{gi} + \\ & (-1)^i \cdot (Z_{mi} - Z_{wi}) \cdot \cos \alpha_0 - \\ & (-1)^i \cdot (X_{mi} - X_{wi}) \cdot \sin \alpha_0 - b_0 - e_i; \end{aligned}$$

$$\begin{aligned} eqs_2 = & -R_p \cdot \theta_{pi} - R_g \cdot \theta_{gi} + \\ & (-1)^i \cdot (Z_{mi} - Z_{wi}) \cdot \cos \alpha_0 + \\ & (-1)^i \cdot (X_{mi} - X_{wi}) \cdot \sin \alpha_0 + b_0 + e_{ri}, \end{aligned}$$

where: R_k , θ_{ki} represent the base circle radius of the gears and their rotational displacements, respectively; subscript k refers to the pinion ($k = p$) or the gear ($k = g$); Z_m , Z_w are the vertical displacements of the motor/pinion and the wheelset/gear, respectively; X_m , X_w are the corresponding longitudinal displacements; b_0 denotes half of the gear backlash; α_0 is the pressure angle of the gear pair; e , e_r are the gear errors for the FSC and BSC, respectively.

It can be seen in Figure 2b that the amplitude and the direction of the mesh force will change when the BSC happens, which may cause impact and vibrations to the gear pair. The mesh force F_m along LOA for FSC and the BSC can be calculated as:

$$F_m = K_{mi} \cdot \delta + C_{mi} \cdot \dot{\delta}, \quad (7)$$

where: K_m , C_m denote the mesh stiffness/damping for the gear teeth engagement; i in the subscript refers to the gear teeth FSC ($i = f$) or the BSC ($i = b$), respectively; $\dot{\delta}$ indicates its 1st order differential of deformation. It is reported by Chen *et al.* (2012) that for the FSC and the BSC of gear teeth, there usually exists a phase difference between their mesh stiffness curves. For the dynamic simulation of the locomotive, the method presented by Chen *et al.* (2012) is also employed in this paper to reveal the phase difference.

In the field of the gear dynamics, time-varying mesh stiffness is one of the most significant excitations inherited by the gear transmissions, which has drawn a vast attentions from the researchers worldwide. Variations of the mesh stiffness are mainly due to the change in the number of the tooth pairs in mesh and the moving of the mesh position along the involute tooth profile. In this paper, the time-varying mesh stiffness, namely K_m in Equation (7),

is calculated by using the analytical model proposed by Chen and Shao (2011, 2013), which is based on the potential energy theory. It is given as:

$$K_m = \frac{\sum_{j=1}^N K_j}{1 + \sum_{j=1}^N \frac{K_j \cdot E_{ij}}{F_m}}, \quad (8)$$

where: N denotes the number of tooth pairs in mesh; F_m is the total mesh force of the gear pair; E_{ij} is the general error function of the gears; i is determined by the tooth pair number whose flexible deformation δ is greatest at an instant time; K_j denotes the single-sided tooth mesh stiffness of the j th tooth pair. The gear tooth stiffness can be calculated by regarding it as a non-uniformly distributed cantilever beam, which is calculated as (Chen, Shao 2011, 2013):

$$K_j = \frac{1}{\frac{1}{K_{t1}} + \frac{1}{K_{f1}} + \frac{1}{K_{t2}} + \frac{1}{K_{f2}} + \frac{1}{K_h}}, \quad (9)$$

where: the symbols K_p , K_f represent the tooth stiffness and the fillet-foundation stiffness, respectively (the numbers in the subscripts refer to the pinion and the gear, respectively); K_h represents the Hertzian contact stiffness.

It should be noted in Equation (6) that the mesh force of the gear pair is affected not only by the rotational motions of the gear pair, but also by the vertical and longitudinal motions of the motor and the wheelset. While the variations of the mesh force will in reverse change the rotational and the lateral motions. Thus, the torsional motions of the mechanical transmission are coupled with the vertical and the longitudinal motions of the locomotive components through the gear mesh interface. Similarly, it can be seen from Equations (1)–(5) that the longitudinal wheel–rail creep forces, which act as the load to the mechanical transmission system are directly determined by the wheel–rail contact, where the rotational, the vertical, and the longitudinal motions of the wheels and the vertical motions of the rail are involved. That is to say, the motions of the mechanical transmission, the vertical and the longitudinal motions, and the rail vertical motions are coupled together. This completely coupled dynamics model enables a more practical dynamic simulation of locomotives under multiple excitations, such as the rail corrugations and the time-varying gear mesh stiffness.

1.3. Numerical integration algorithm

There are many nonlinear factor and time-varying parameters considered in this dynamics model. Thus, analytical method is nearly impossible for solving such a large-scale dynamics model. Therefore, numerical integration method is essential for this problem. In this study, a fast explicit and effective numerical integration algorithm called Zhai method (Zhai 1996) is adopted. It has an integration form

shown as follows:

$$\begin{cases} \mathbf{X}_{n+1} = \mathbf{X}_n + \dot{\mathbf{X}}_n \cdot \Delta t + (0.5 + \psi) \cdot \ddot{\mathbf{X}}_n \cdot \Delta t^2 - \psi \cdot \ddot{\mathbf{X}}_{n-1} \cdot \Delta t^2; \\ \dot{\mathbf{X}}_{n+1} = \dot{\mathbf{X}}_n + (1 + \phi) \cdot \ddot{\mathbf{X}}_n \cdot \Delta t - \phi \cdot \ddot{\mathbf{X}}_{n-1} \cdot \Delta t, \end{cases} \quad (10)$$

where: \mathbf{X} , $\dot{\mathbf{X}}$, $\ddot{\mathbf{X}}$ are the displacement/velocity/acceleration vectors indicating the motions of the system; ψ , ϕ are the free parameters that control the stability and numerical dissipation of the algorithm (a value of 0.5 is suggested by Zhai (1996) for both of the 2 free parameters to achieve a good compatibility between numerical stability and accuracy); Δt is the time step; n denotes the instant time at $n \cdot \Delta t$.

2. Dynamic simulation and result discussions

The dynamic responses of the locomotive can be calculated based on the developed locomotive-track coupled dynamics model where the torsional motions of the geared mechanical transmission system are considered. The main design parameters of the locomotive used in the simulation of this study are the same as that in the work done by Chen *et al.* (2017b), which are also shown here in Table 1. In addition, the main design parameters of the gear transmission system are also from the same work, namely that done by Chen *et al.* (2017b), which are also shown in Table 2. In addition, the dry rail surface condition obtained from the China railway lines is adopted where the

values of the coefficients in Equation (2) are given as: $a = 0.53$, $b = 0.12$, $c = 0.53$, and $d = 2.40$. Thus the curve of the adhesion coefficient can be drawn which is shown in Figure 3 from which it can be observed that the maximum value of the adhesion coefficient can be reached at the relative slip velocity of 0.365 m/s. Running speed of the locomotive is 100 km/h in this dynamic simulation at which speed this locomotive is usually operating in practice. Time-varying mesh stiffness is a very significant excitation in the geared mechanical transmissions. In this study, it is calculated by using Equations (8) and (9), and displayed in Figure 3. It can be seen that the mesh stiffness is varying periodically between the single- and the double-sided tooth engagements due to variation of the number of the tooth pairs in mesh. The other excitation, namely the rail corrugation, is represented by sinusoidal waveform, which has the following form as:

$$Z_0(t) = A \cdot \sin\left(\frac{2 \cdot \pi \cdot x}{L} + \psi\right), \quad (11)$$

where: A , ψ , L represent the amplitude, the phase and the wavelength of the rail corrugation, respectively; x denotes the longitudinal displacement of the wheelset. In this study, the phase ψ is assumed to be zero. The simulation scenarios include various rail corrugations with different wavelength and amplitude, namely the wavelength varies from 0 to 5 m, and the amplitude from 0 to 1 mm.

Table 1. Main design parameters of the locomotive for simulation

Notation	Specification	Value
M_c	car body mass [kg]	$6.26 \cdot 10^4$
J_c	mass moment of inertia of car body [$\text{kg} \cdot \text{m}^2$]	$1.434 \cdot 10^6$
M_t	bogie mass [kg]	$6.275 \cdot 10^3$
J_t	mass moment of inertia of bogie frame [$\text{kg} \cdot \text{m}^2$]	$1.311 \cdot 10^4$
M_w	wheelset mass [kg]	$2.77 \cdot 10^3$
J_w	mass moment of inertia of wheelset [$\text{kg} \cdot \text{m}^2$]	$1.081 \cdot 10^3$
M_m	motor mass [kg]	$2.66 \cdot 10^3$
J_m	mass moment of inertia of motor [$\text{kg} \cdot \text{m}^2$]	$4 \cdot 10^2$
K_{pz}	stiffness of primary suspension [N/m]	$3.14 \cdot 10^6$
C_{pz}	damping coefficient of primary suspension [N·s/m]	$5 \cdot 10^4$
K_{sz}	stiffness of secondary suspension [N/m]	$2.14 \cdot 10^6$
C_{sz}	damping coefficient of secondary suspension [N·s/m]	$9 \cdot 10^4$
K_{ms}	stiffness of suspension connecting motor and bogie frame [N/m]	$3 \cdot 10^6$
C_{ms}	damping coefficient of suspension connecting motor and bogie frame [N·s/m]	$1.0 \cdot 10^2$
K_{br}	stiffness of axle-hung bearing supporting motor on wheel axle [N/m]	$1.0 \cdot 10^8$
C_{br}	damping coefficient of axle-hung bearing supporting motor on wheel axle [N·s/m]	$1.0 \cdot 10^3$
K_{pr}	tractive rod stiffness of primary suspension [N/m]	$1.645 \cdot 10^8$
K_{sr}	tractive rod stiffness of secondary suspension [N/m]	$1.0 \cdot 10^8$
l_c	semi-longitudinal distance between bogies [m]	5.03
l_t	semi-longitudinal distance between wheelsets in bogie [m]	1.3
l_{s1}	longitudinal distance between bogie center and hung position of motor on bogie [m]	0.274
l_{s2}	longitudinal distance between pinion center and hung position of motor on bogie [m]	0.45
l_{s3}	distance between centers of pinion and gear [m]	0.576
R_0	wheel radius [m]	0.625

Table 2. Main design parameters of the gear transmission system

Notation	Specification	Value	
		pinion	gear
–	material	steel	
–	tooth shape	involute	
m	module [mm]	8	
α_0	pressure angle [°]	20	
β	helical angle [°]	0	
b_c	tooth backlash [μm]	10	
h_a^*	addendum coefficient	1	1
c_n^*	tip clearance coefficient	0.25	0.25
Z	number of teeth	23	120
W	face width [mm]	175	136
X_n	tooth profile shift coefficient	0.362	0.151

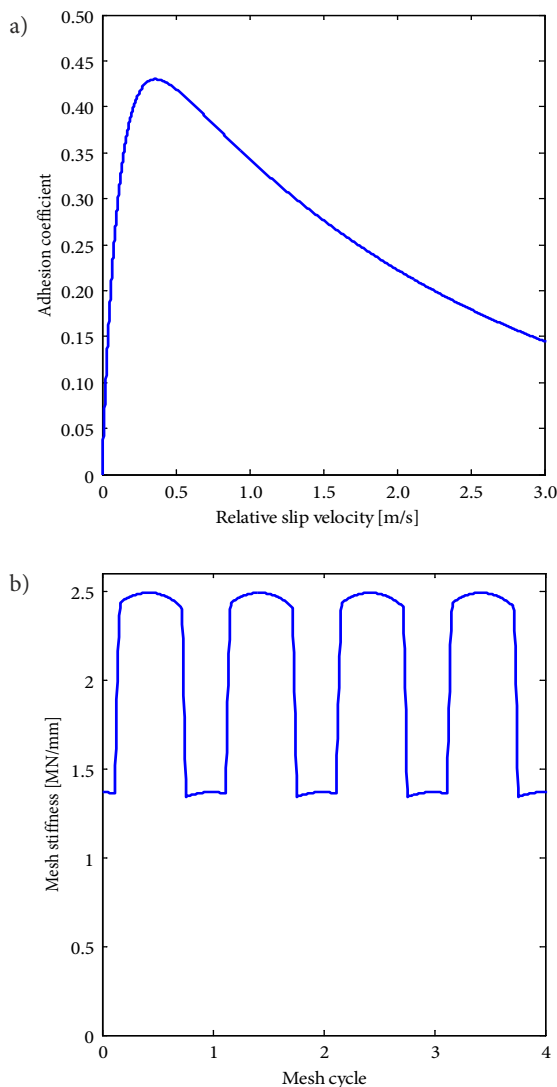


Figure 3. Dynamic excitations: a – wheel–rail adhesion coefficient; b – time-varying gear mesh stiffness

The initial values for the dynamic simulation are given as: (1) the initial displacements for all the DOFs are assigned with the ones under the static equilibrium conditions of the dynamics system; and (2) the initial velocities for all the DOFs are given as zero except the rotational motions of the mechanical transmission system and the longitudinal motions of all the components, which are calculated from the prescribed locomotive running speed. It should be noted that the results presented in this paper are extracted from the ones corresponding to the steady state where the oscillations caused by the initial disturbance are excluded.

Dynamic responses of the locomotive–track coupled dynamics system are obtained by simulation under the excitations from both the rail corrugation and the time-varying gear mesh stiffness. The corresponding results with 4 wavelengths, namely 0.5, 1, 2, and 4 m, are extracted out and exhibited in Figures 4–10. The time histories and the frequency spectrums of the vibration accelerations of the 1st wheelset are shown in Figure 4. Note that the displaying ranges of the vertical coordinates are not adjusted to be the same for the 4 cases in order for better clarification. The vertical coordinates of the frequency spectrum are displayed in logarithm form.

The vertical vibration acceleration responses of the 1st wheelset are presented in Figure 4. It can be seen that the time histories and the corresponding frequency spectrums exhibit apparent discrepancies between them. That is to say different rail corrugation is likely to cause completely different vibration responses of locomotives. The low frequency vibrations of the wheelset are dominated by the rail corrugation excitations. Among the 4 cases, the wheelset vibration is most sensitive to the rail corrugation with wavelength of 1 m, which is displayed in Figure 4b. For this case, the time history of the vibration appears to be random and impulsive compared with the other 3 cases, and the corresponding frequency spectrum shows a relative higher vibration level in the entire frequency range shown. In addition, the mesh frequency and its harmonics can hardly be found in this case. The time histories of the other 3 cases, namely that in Figures 4a, 4c and 4d, are more regular than that in Figure 4b. This observation agrees well with the conclusion obtained by Andersson and Johansson (2004) that a high corrugation growth rate may appear at certain wavelengths corresponds to specific excited vibrational modes of the coupled train–track system. In this study, the rail corrugation with wavelength of 1 m is much more possible to grow fast than other 3 cases due to the more severe wheel–rail interactions, which should be concerned for the rail grinding work. What’s more, the phenomenon that the high frequency vibrations with respect to gear mesh process are modulated by the low frequency vibrations caused by the rail corrugations, where the chaotic vibrations case is an exception.

The corresponding phase diagrams of the wheelset vibration for the 4 cases are shown in Figure 5. It can be seen that the wheelset vibrates with a periodic motion

when the corrugation wavelength is 0.5 m. While its motion will move into a chaotic state when the corrugation wavelength is 1 m. When the corrugation wavelength is 2 m, vibration of the wheelset will become to be a period-doubling bifurcation, and then it will be back to the periodic motion state when the corrugation wavelength is 4 m. It indicates that this large-scale and complicated locomotive-track coupled dynamics system will exhibit abundant nonlinear motion postures under multiple excitations, such as the rail corrugations and the time-varying mesh stiffness.

Similarly, the dynamic vibration of the motor is also extracted and shown in Figures 6 and 7. Compared with the vibration response of the wheelset, the motor vibrations have the similar tendency and profile for the time histories and the frequency spectrum as well as the phase diagrams. This is due to the same excitations from the rail corrugations and the time-varying mesh stiffness.

Meanwhile, the time histories of the DTE of the 1st gear transmission and the corresponding frequency spectrums are presented in Figure 8, where it can be seen that

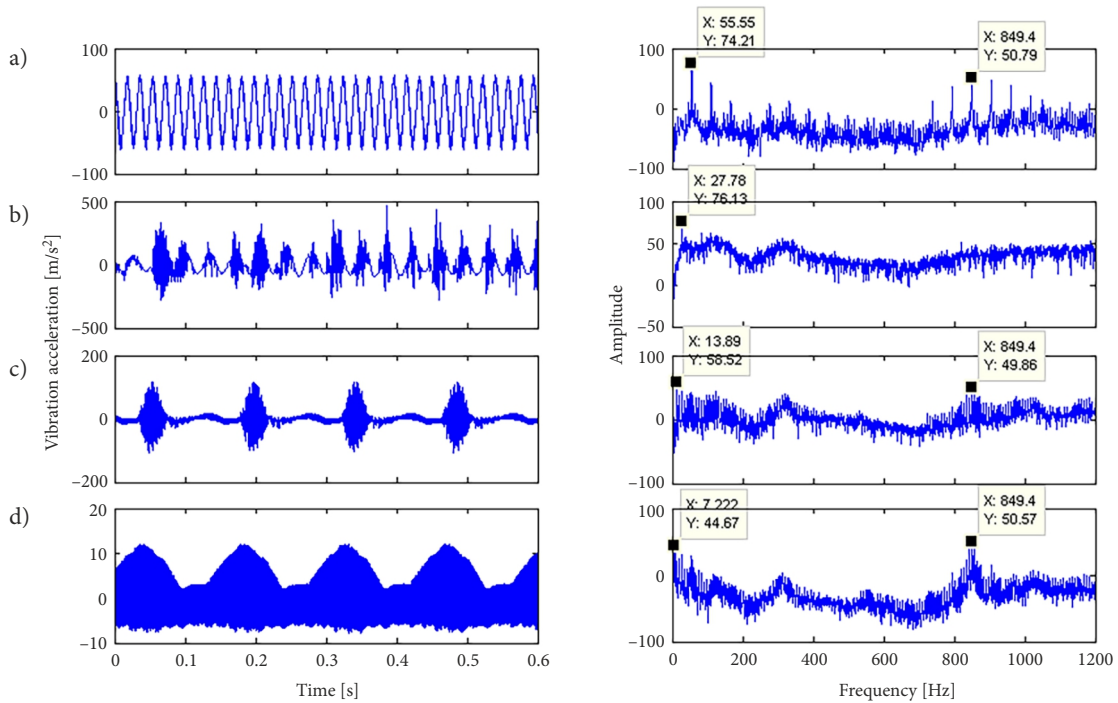


Figure 4. Vertical vibration acceleration of the 1st wheelset under rail corrugation excitations with $A = 1$ mm: a - $L = 0.5$ m; b - $L = 1$ m; c - $L = 2$ m; d - $L = 4$ m

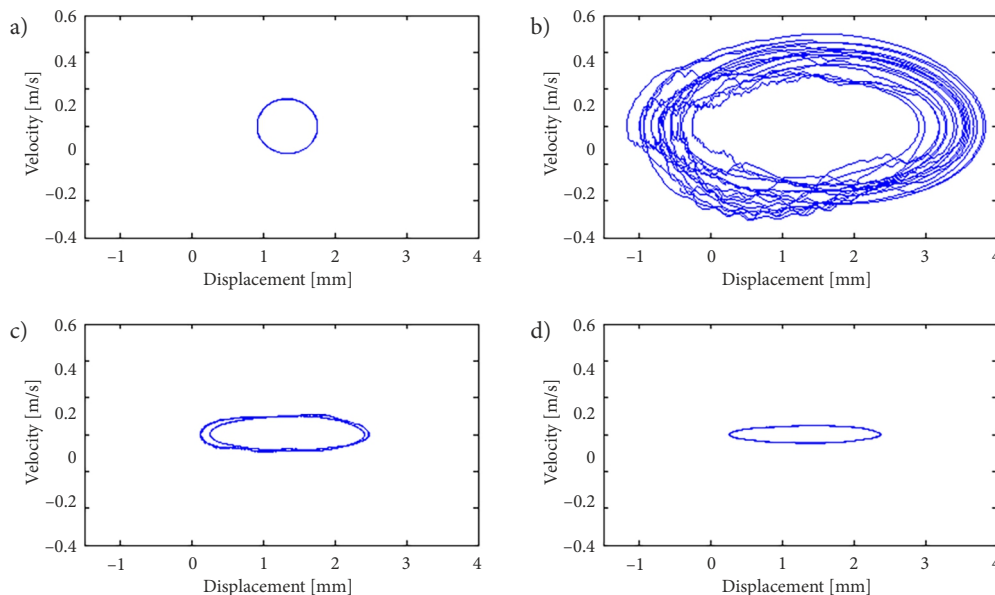


Figure 5. Phase diagram of the 1st wheelset under rail corrugation excitations with $A = 1$ mm: a - $L = 0.5$ m; b - $L = 1$ m; c - $L = 2$ m; d - $L = 4$ m

the similar phenomenon can be observed. However, more direct reasons can be found for illustration on the complicated nonlinear dynamic responses shown in Figures 4 to 7. For the chaotic case, namely the dynamic responses when excited by the rail corrugation with wavelength of 1 m, the DTE appears to be random. The apparent tooth contact loss or even the serious double-sided tooth contact happens to the gear transmission system. These irregular impulsive forces are likely to cause the chaotic vibrations of the locomotive–track coupled dynamics system. It can be also observed in Figure 8c that the bifurcation vibrations

of the system aforementioned are caused by the great oscillations of the mesh forces derived from the DTE results, which is caused by the tooth contact loss. In this case, the gear teeth impact also happens to the gear pair, but with a smaller severity than the double-sided tooth contact observed in Figure 8b. Besides, it can be clearly seen in Figure 8 that the periodic motions are observed under the conditions that without gear tooth contact loss, namely the 2 cases where the rail corrugation wavelengths are 0.5 m and 4 m, respectively. The phase diagrams of the gear transmission responses for the 4 cases are given in Figure 9.

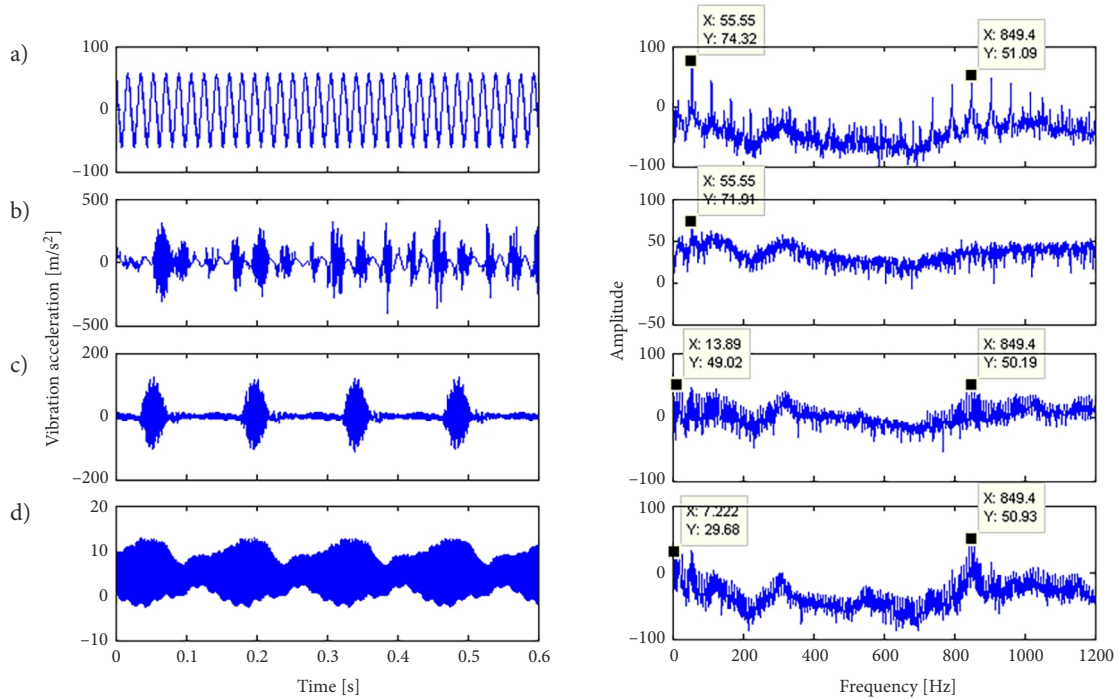


Figure 6. Vertical vibration acceleration of the 1st motor under rail corrugation excitations with $A = 1$ mm: a - $L = 0.5$ m; b - $L = 1$ m; c - $L = 2$ m; d - $L = 4$ m

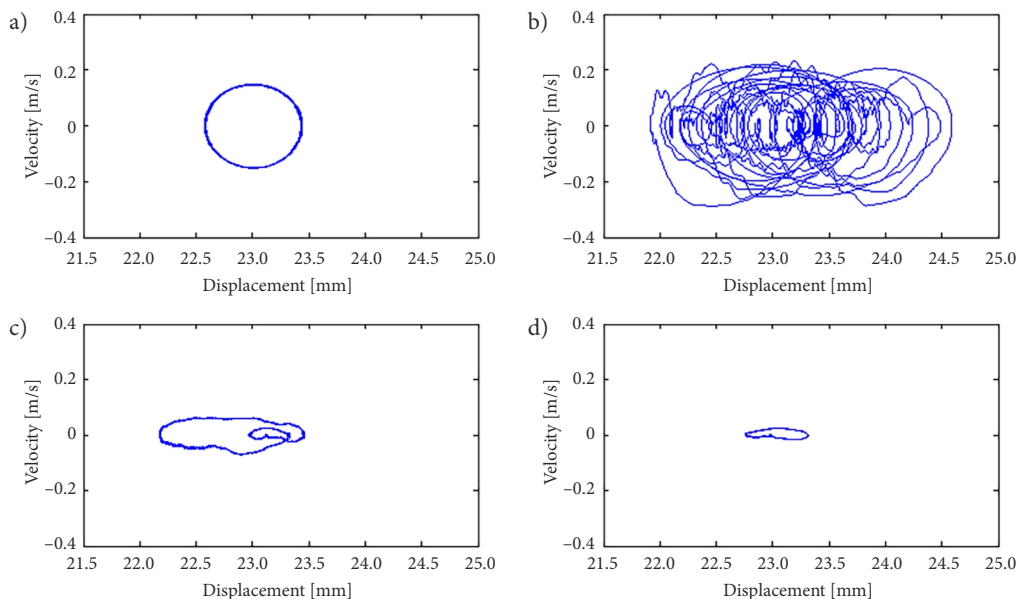


Figure 7. Phase diagram of the 1st motor under rail corrugation excitations with $A = 1$ mm: a - $L = 0.5$ m; b - $L = 1$ m; c - $L = 2$ m; d - $L = 4$ m

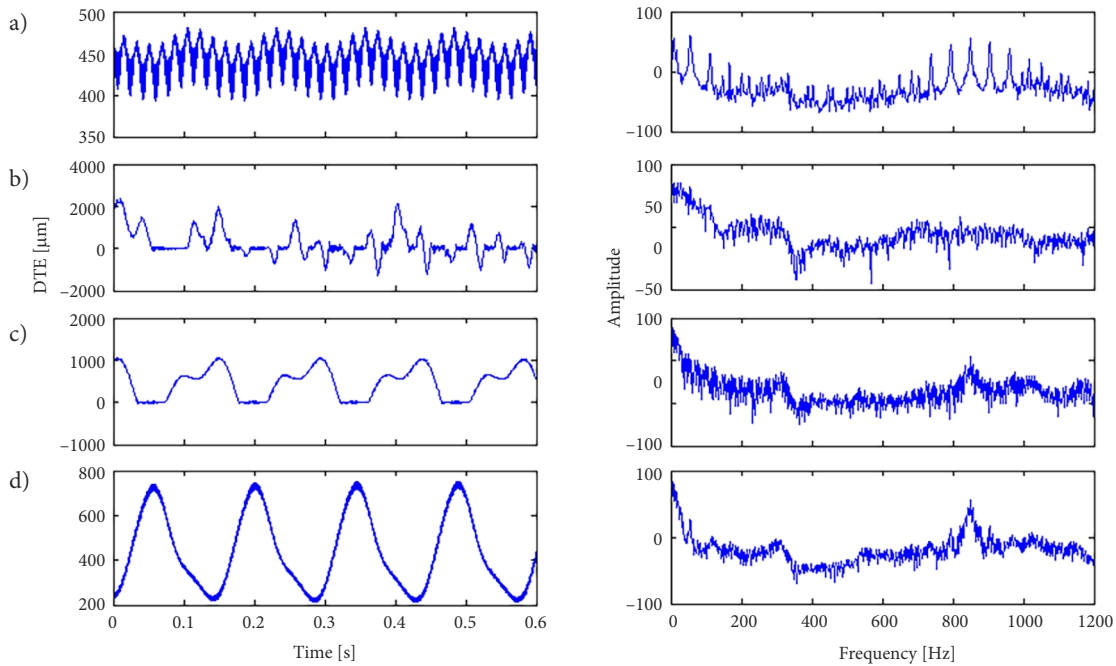


Figure 8. DTE of the 1st gear transmission under rail corrugation excitations with $A = 1$ mm:
a - $L = 0.5$ m; b - $L = 1$ m; c - $L = 2$ m; d - $L = 4$ m

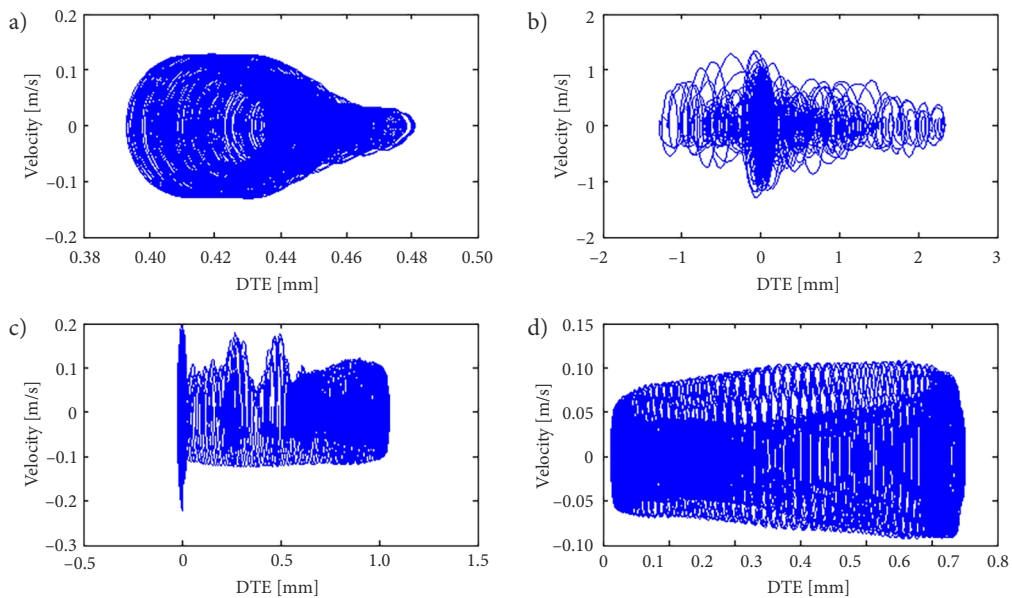


Figure 9. Phase diagram of the 1st gear transmission under rail corrugation excitations with $A = 1$ mm:
a - $L = 0.5$ m; b - $L = 1$ m; c - $L = 2$ m; d - $L = 4$ m

The time histories of the wheelset longitudinal relative slip velocity are displayed in Figure 10. It can be seen that the 3 cases shown in Figures 10a, 10c and 10d respectively have the similar variation amplitude of the slip velocity but with different waveforms. The discrepancies in the waveforms will change the longitudinal creep forces thus leading to variations of the system vibration responses. The 2 cases shown respectively in Figures 10a and 10c have the similar phase shift between the slip velocity and the rail corrugation, where the maximum slip velocity usually happens near the valley zone of the rail corrugation, which is likely to accelerate propagation of

the rail corrugation. While the case shown in Figure 10d with rail corrugation wavelength of 4 m has an opposite phase between the slip velocity and the rail corrugation, indicating the maximum slip velocity appears at the wave crest of the rail corrugation. This type of corrugation may be reduced after a long time operation of the locomotive at the specified running speed. Again, the highly concerned rail corrugation case is shown in Figure 10b. It can be seen that the slip velocity varies in a larger amplitude from positive to negative. The locomotive vibrations are more sensitive to the rail corrugation with this wavelength. While in reverse, these serious oscillations will be likely to

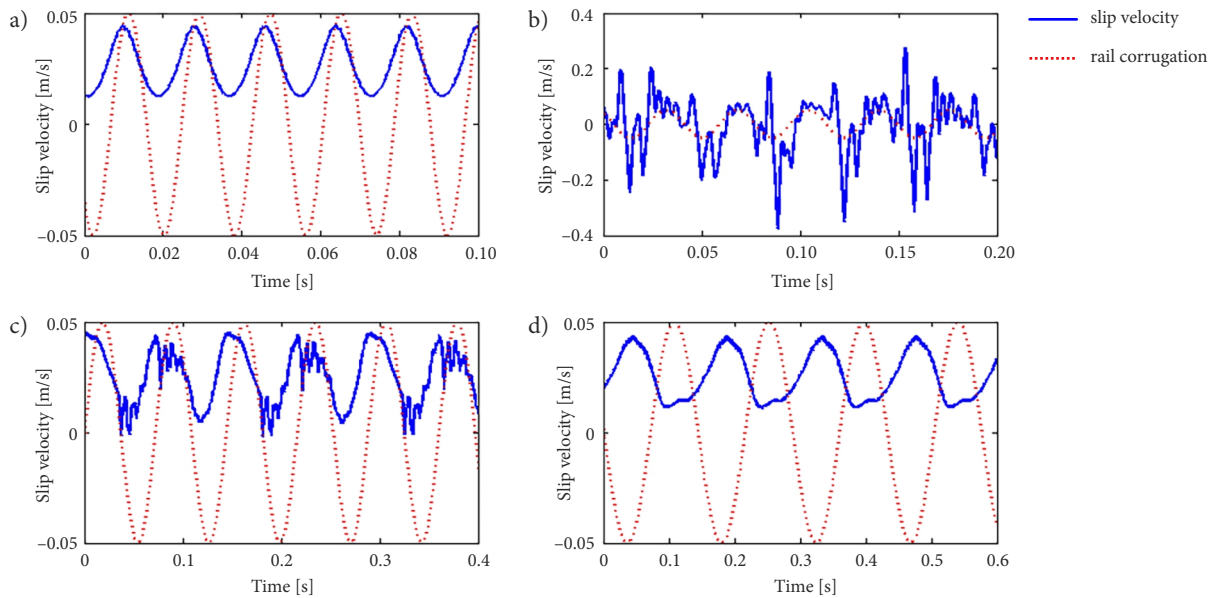


Figure 10. Time history of the wheel–rail longitudinal slip velocity under rail corrugation excitations with $A = 1$ mm: a – $L = 0.5$ m; b – $L = 1$ m; c – $L = 2$ m; d – $L = 4$ m

accelerate the propagation of the rail corrugations. It should be noted that the rail corrugation curves are also shown in Figures 10–13 by ignoring their actual amplitude for better observation, where the positive peak denotes the trough of the corrugation.

Additionally, the wheelset vertical vibration, wheel–rail slip velocity, and the DTE of gear transmissions are presented in Figures 11–13 to reveal the difference between dynamic responses of different wheelsets. It can be seen that the uniform periodic motions appear for the smaller corrugation amplitude, while the motions will move into the chaotic status when the corrugation amplitude increases to a certain value due to the serious wheel–rail impacts. For both the 2 presented corrugation amplitudes, there exist apparent discrepancies in the dynamic responses (including both the amplitude and the phase relative to the corrugation) between wheelset 1 and 4. Actually, wheelset 1 and 3 (or wheelset 2 and 4) have the similar dynamic responses with each other although they are not displayed here.

While for the DTE of gear transmissions shown in Figure 13, the results between wheelset 1 and 4 have very small difference when no wheel–rail impact happens, however, there seems no determinate law could be found when the wheel–rail impact phenomenon is present. These differences in the dynamic responses between different wheelset are believed to be caused by the coupling effect of the components motions through the primary and the secondary suspension elements due to the involvement of mechanical transmission system, which will cause load transfer between the different wheelsets and bogies. Consequently, using more complete locomotive coupling dynamics model considering power transmission system could assist making more precise prediction of rail corrugation evolution.

In order for investigation on the effect of the rail corrugation, a wider range of the amplitude and the wavelength is selected for simulation, namely the wavelength varies from 0.02 m to 5 m and the amplitude from 0 to 1 mm. The statistical indicator, namely the RMS (Chen, Shao 2011), is used to reveal the vibration level of the locomotive components under the excitations of the rail corrugation with different wavelength and amplitude. The results with respect to the vibrations of the motor, the wheelset, and the gear transmission are given out and shown in Figures 14–16, respectively. In general, the RMS results in the 3 figures have the similar tendency versus the rail corrugation amplitude and the wavelength. The vibration level increases generally with the growth of the rail corrugation amplitude, however, it appears to be more sensitive to the rail corrugations with specific wavelength, such as 0.3 m and 1 m in this study. Vibrations of the wheelset and the motor are much less sensitive to the rail corrugation when the wavelength is larger than 2 m for the studied conditions, however, some sensitive rail corrugation wavelengths can be also found. Some discrepancies in the results between wheelset 1 and 4 can be also found under some corrugation conditions.

While for the RMS results of the DTE of the gear transmission shown in Figure 16, much more complicated vibration variations with different amplitude and wavelength of rail corrugation are observed. Some resonance vibration ranges can also be found. The complexity of the gear vibration variation may be due to the multiple excitations (e.g., rail corrugation and time-varying mesh stiffness) and the nonlinear factors (gear tooth backlash and nonlinear wheel–rail contact). It is shown that some specific rail corrugations will bring drastic dynamic excitations to the geared mechanical transmission system in a locomotive, which should be avoided so as for failure preventions.

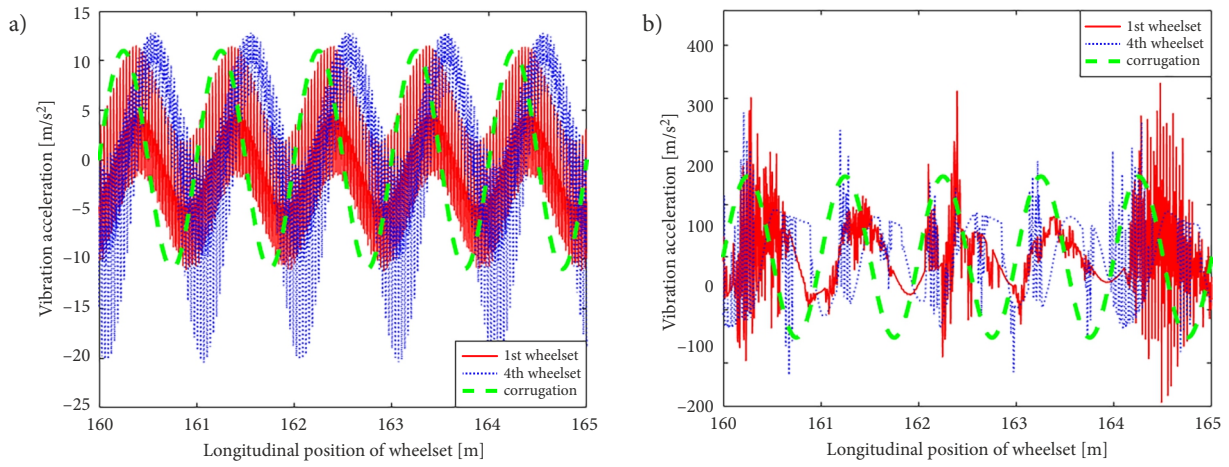


Figure 11. Wheelset vertical vibration under rail corrugation excitation with $L = 1$ m: a - $A = 100 \mu m$; b - $A = 1000 \mu m$

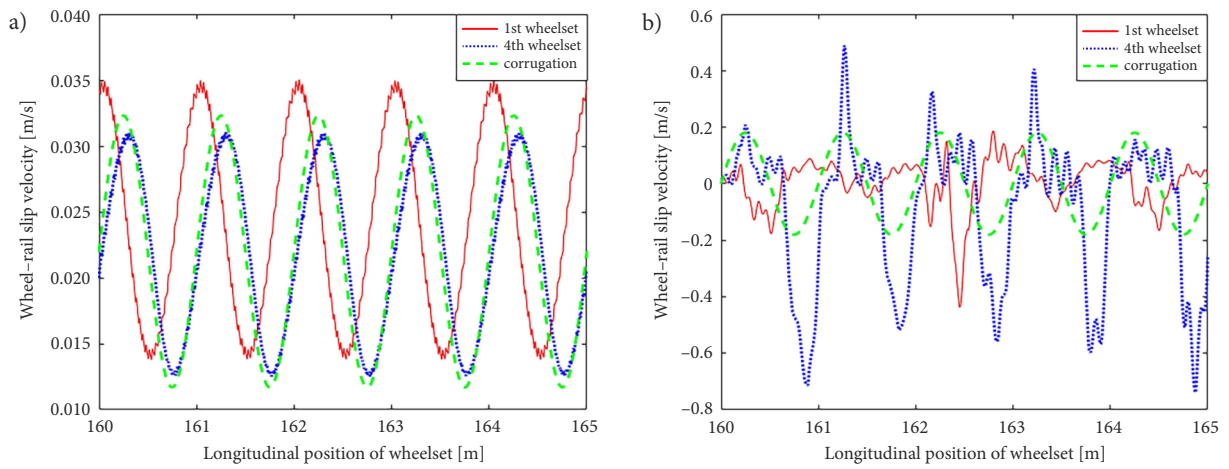


Figure 12. Wheel-rail slip velocity under rail corrugation excitation with $L = 1$ m: a - $A = 100 \mu m$; b - $A = 1000 \mu m$

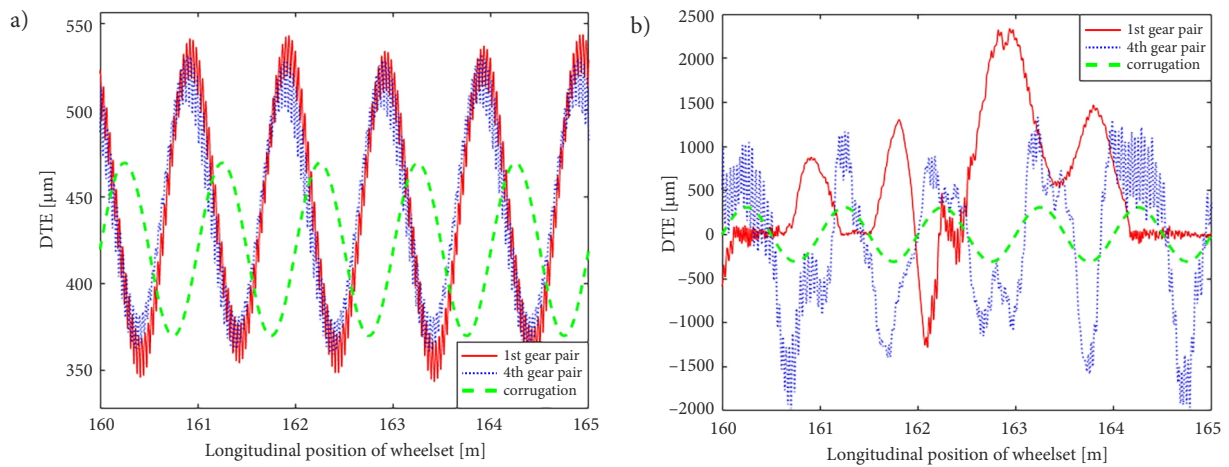


Figure 13. Gear DTEs under rail corrugation excitation with $L = 1$ m: a - $A = 100 \mu m$; b - $A = 1000 \mu m$

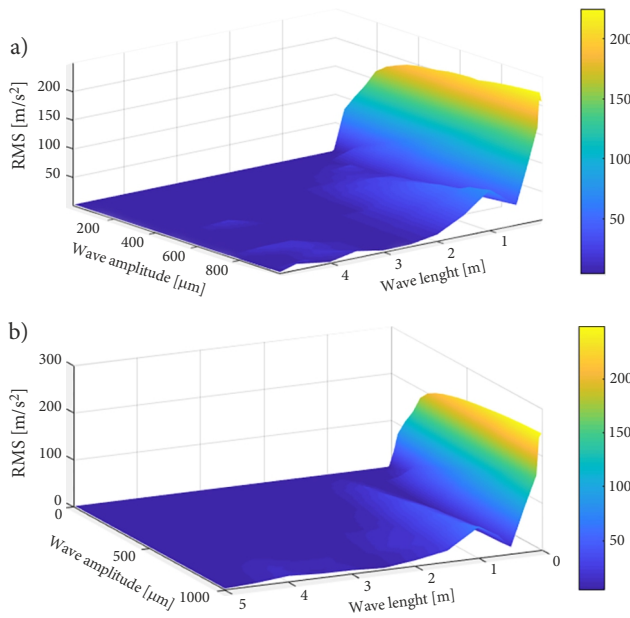


Figure 14. RMS values of the vertical vibration accelerations for: a – the 1st wheelset; b – the 4th wheelset

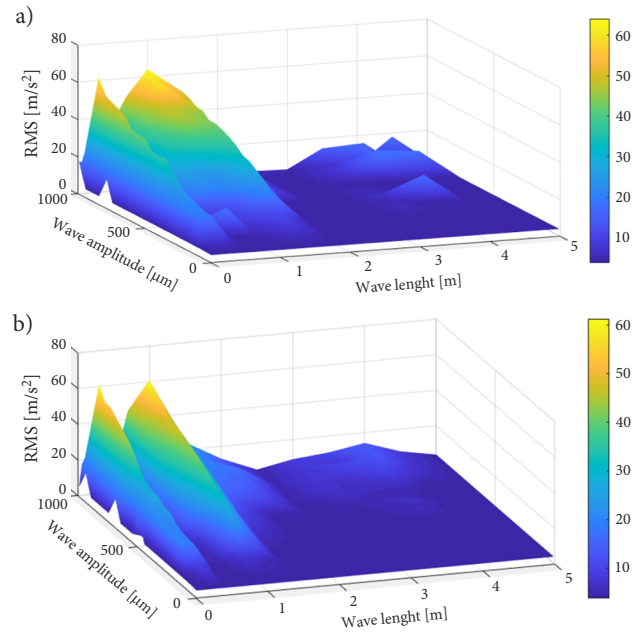


Figure 15. RMS values of the vertical vibration accelerations for the motor mounted on: a – the 1st wheelset; b – the 4th wheelset

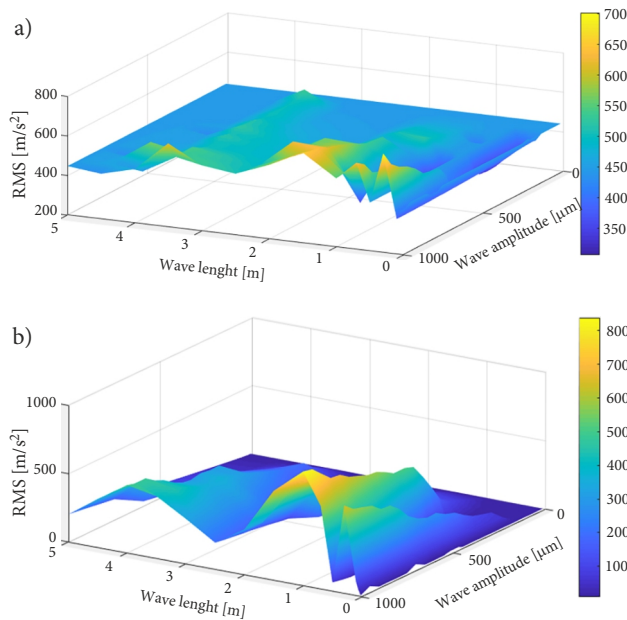


Figure 16. RMS values of the DTE for gear transmissions on: a – the 1st wheelset; b – the 4th wheelset

Conclusions

A locomotive–track coupled dynamics model with effect of gear transmissions in our previous work is employed in this paper for dynamic investigations. In this model, the torsional vibration of the geared mechanical transmissions, the vertical and the longitudinal motions of the locomotive, and the vertical vibration of the track structure are taken into consideration. Based on this coupled dynamics model, the nonlinear dynamic responses of this dynamics system are analysed under the excitations from the time-varying mesh stiffness and the rail corrugations with dif-

ferent wavelength and amplitude. The results indicate that the vibration level of the locomotive components generally increase with the growth of the corrugation amplitude, while, it is much more sensitive to some rail corrugations with specific wavelength. This is meaningful for offering some theoretical guidance on making proper rail grinding schedule. Meanwhile, the high frequency vibrations are mainly dominated by the time-varying mesh stiffness, while the low frequency vibrations usually dominated by the rail corrugations. A modulation phenomenon of the gear mesh frequency related vibrations by the rail corrugation related vibrations is observed in the simulated results except for the chaotic cases, which are mainly caused by the wheel–rail impacts. Additionally, the bifurcation and chaotic phenomenon appear when the dynamics system is being excited by the sensitive rail corrugations, while the periodic vibrations are usually observed for the non-sensitive rail corrugations. Besides, some discrepancies in the dynamic responses between different wheelsets are observed which is caused by the load transfer due to involvement of the gear transmission systems. This more detailed locomotive dynamics model is thus suggested for more precise rail corrugation prediction, of course, more detailed and accurate wheel–rail contact model should be included.

It should be noted that, there are also some works remained to be further investigated. Such as, the effect from the lateral motions, the lateral and roll track irregularities could not be considered by using the developed 2D dynamics model; the interactions between the mechanical and electrical systems are neglected; and the detailed wheel–rail contact modelling has not been included which is essential if the initiation and evolution process of the rail corrugation are focused.

References

- Andersson, C.; Johansson, A. 2004. Prediction of rail corrugation generated by three-dimensional wheel–rail interaction, *Wear* 257(3–4): 423–434. <https://doi.org/10.1016/j.wear.2004.01.006>
- Chaari, F.; Fakhfakh, T.; Haddar, M. 2009. Analytical modelling of spur gear tooth crack and influence on gearmesh stiffness, *European Journal of Mechanics – A/Solids* 28(3): 461–468. <https://doi.org/10.1016/j.euromechsol.2008.07.007>
- Chen, Z.; Shao, Y. 2011. Dynamic simulation of spur gear with tooth root crack propagating along tooth width and crack depth, *Engineering Failure Analysis* 18(8): 2149–2164. <https://doi.org/10.1016/j.engfailanal.2011.07.006>
- Chen, Z.; Shao, Y. 2013. Mesh stiffness calculation of a spur gear pair with tooth profile modification and tooth root crack, *Mechanism and Machine Theory* 62: 63–74. <https://doi.org/10.1016/j.mechmachtheory.2012.10.012>
- Chen, Z. G.; Shao, Y. M.; Lim, T. C. 2012. Non-linear dynamic simulation of gear response under the idling condition, *International Journal of Automotive Technology* 13(4): 541–552. <https://doi.org/10.1007/s12239-012-0052-1>
- Chen, Z.; Zhai, W.; Shao, Y.; Wang, K.; Sun, G. 2016. Analytical model for mesh stiffness calculation of spur gear pair with non-uniformly distributed tooth root crack, *Engineering Failure Analysis* 66: 502–514. <https://doi.org/10.1016/j.engfailanal.2016.05.006>
- Chen, Z.; Zhai, W.; Wang, K. 2017a. A locomotive–track coupled vertical dynamics model with gear transmissions, *Vehicle System Dynamics: International Journal of Vehicle Mechanics and Mobility* 55(2): 244–267. <https://doi.org/10.1080/00423114.2016.1254260>
- Chen, Z.; Zhai, W.; Wang, K. 2017b. Dynamic investigation of a locomotive with effect of gear transmissions under tractive conditions, *Journal of Sound and Vibration* 408: 220–233. <https://doi.org/10.1016/j.jsv.2017.07.017>
- Chen, Z.; Zhang, J.; Zhai, W.; Wang, Y.; Liu, J. 2017c. Improved analytical methods for calculation of gear tooth fillet-foundation stiffness with tooth root crack, *Engineering Failure Analysis* 82: 72–81. <https://doi.org/10.1016/j.engfailanal.2017.08.028>
- Correa, N.; Oyarzabal, O.; Vadillo, E. G.; Santamaria, J.; Gomez J. 2011. Rail corrugation development in high speed lines, *Wear* 271(9–10): 2438–2447. <https://doi.org/10.1016/j.wear.2010.12.028>
- Grassie, S. L. 2009. Rail corrugation: characteristics, causes, and treatments, *Proceedings of the Institution of Mechanical Engineers, Part F: Journal of Rail and Rapid Transit* 223(6): 581–596. <https://doi.org/10.1243/09544097JRR264>
- Grassie, S. L.; Kalousek, J. 1993. Rail corrugation: characteristics, causes and treatments, *Proceedings of the Institution of Mechanical Engineers, Part F: Journal of Rail and Rapid Transit* 207(1): 57–68. https://doi.org/10.1243/PIME_PROC_1993_207_227_02
- Ishikawa, Y.; Kawamura, A. 1997. Maximum adhesive force control in super high speed train, in *Proceedings of Power Conversion Conference – PCC'97*, 6 August 1997, Nagaoka, Japan, 2: 951–954. <https://doi.org/10.1109/PCCON.1997.638382>
- Iwnicki, S. 2003. Simulation of wheel–rail contact forces, *Fatigue & Fracture of Engineering Materials & Structures* 26(10): 887–900. <https://doi.org/10.1046/j.1460-2695.2003.00699.x>
- Kalker, J. J.; Piotrowski, J. 1989. Some new results in rolling contact, *Vehicle System Dynamics: International Journal of Vehicle Mechanics and Mobility* 18(4): 223–242. <https://doi.org/10.1080/00423118908968920>
- Li, S.; Li, Z.; Núñez, A.; Dollevoet, R. 2017. New insights into the short pitch corrugation enigma based on 3D-FE coupled dynamic vehicle-track modeling of frictional rolling contact, *Applied Sciences* 7(8): 807. <https://doi.org/10.3390/app7080807>
- Liang, X.; Zuo, M. J.; Pandey, M. 2014. Analytically evaluating the influence of crack on the mesh stiffness of a planetary gear set, *Mechanism and Machine Theory* 76: 20–38. <https://doi.org/10.1016/j.mechmachtheory.2014.02.001>
- Ling, L.; Li, W.; Shang, H.; Xiao, X.; Wen, Z.; Jin, X. 2014. Experimental and numerical investigation of the effect of rail corrugation on the behaviour of rail fastenings, *Vehicle System Dynamics: International Journal of Vehicle Mechanics and Mobility* 52(9): 1211–1231. <https://doi.org/10.1080/00423114.2014.934844>
- Ma, H.; Zeng, J.; Feng, R.; Pang, X.; Wang, Q.; Wen, B. 2015. Review on dynamics of cracked gear systems, *Engineering Failure Analysis* 55: 224–245. <https://doi.org/10.1016/j.engfailanal.2015.06.004>
- Matsumoto, A.; Sato, Y.; Ono, H.; Tanimoto, M.; Oka, Y.; Miyachi, E. 2002. Formation mechanism and countermeasures of rail corrugation on curved track, *Wear* 253(1–2): 178–184. [https://doi.org/10.1016/S0043-1648\(02\)00097-2](https://doi.org/10.1016/S0043-1648(02)00097-2)
- Polach, O. 2005. Creep forces in simulations of traction vehicles running on adhesion limit, *Wear* 258(7–8): 992–1000. <https://doi.org/10.1016/j.wear.2004.03.046>
- Sainsot, P.; Velez, P.; Duverger, O. 2004. Contribution of gear body to tooth deflections – a new bidimensional analytical formula, *Journal of Mechanical Design* 126(4): 748–752. <https://doi.org/10.1115/1.1758252>
- Sato, Y.; Matsumoto, A.; Knothe, K. 2002. Review on rail corrugation studies, *Wear* 253(1–2): 130–139. [https://doi.org/10.1016/S0043-1648\(02\)00092-3](https://doi.org/10.1016/S0043-1648(02)00092-3)
- Shabana, A. A.; Sany, J. R. 2001. A survey of rail vehicle track simulations and flexible multibody dynamics, *Nonlinear Dynamics* 26(2): 179–210. <https://doi.org/10.1023/A:1012976302105>
- Shao, Y.; Chen, Z. 2013. Dynamic features of planetary gear set with tooth plastic inclination deformation due to tooth root crack, *Nonlinear Dynamics* 74(4): 1253–1266. <https://doi.org/10.1007/s11071-013-1038-x>
- Tian, X. 2004. *Dynamic Simulation for System Response of Gear-box Including Localized Gear Faults*. MSc Thesis. University of Alberta, Edmonton, Alberta, Canada. 109 p. <https://doi.org/10.7939/r3-05s3-by17>
- Wang, K.; Liu, P.; Zhai, W.; Huang, C.; Chen, Z.; Gao, J. 2015. Wheel/rail dynamic interaction due to excitation of rail corrugation in high-speed railway, *Science China Technological Sciences* 58(2): 226–235. <https://doi.org/10.1007/s11431-014-5633-y>
- Weber, C. 1951. *The Deformation of Loaded Gears and the Effect on their Load Carrying Capacity*. Department of Scientific and Industrial Research, London, UK. 111 p.
- Wu, S.; Zuo, M. J.; Parey, A. 2008. Simulation of spur gear dynamics and estimation of fault growth, *Journal of Sound and Vibration* 317(3–5): 608–624. <https://doi.org/10.1016/j.jsv.2008.03.038>

- Yang, D. C. H.; Lin, J. Y. 1987. Hertzian damping, tooth friction and bending elasticity in gear impact dynamics, *Journal of Mechanisms, Transmissions, and Automation in Design* 109(2): 189–196. <https://doi.org/10.1115/1.3267437>
- Zhai, W.-M. 1996. Two simple fast integration methods for large-scale dynamic problems in engineering, *International Journal for Numerical Methods in Engineering* 39(24): 4199–4214. [https://doi.org/10.1002/\(SICI\)1097-0207\(19961230\)39:24<4199::AID-NME39>3.0.CO;2-Y](https://doi.org/10.1002/(SICI)1097-0207(19961230)39:24<4199::AID-NME39>3.0.CO;2-Y)
- Zhai, W.; Sun, X. 1994. A detailed model for investigating vertical interaction between railway vehicle and track, *Vehicle System Dynamics: International Journal of Vehicle Mechanics and Mobility* 23(Suppl 1): 603–615. <https://doi.org/10.1080/00423119308969544>
- Zhai, W.; Wang, K.; Cai, C. 2009. Fundamentals of vehicle–track coupled dynamics, *Vehicle System Dynamics: International Journal of Vehicle Mechanics and Mobility* 47(11): 1349–1376. <https://doi.org/10.1080/00423110802621561>